A case study of the RothC soil carbon model with potential evapotranspiration and remote sensing model inputs

Ellen D.v.L. Maas[a,*], Rattan A. Lal[a]

[a] *School of Environment and Natural Resources, The Ohio State University, 2021 Coffey Road, Columbus, OH 43210, USA*

* Corresponding author.

Email addresses: alaskabasin@gmail.com (E.D.v.L. Maas), lal.1@osu.edu (R. Lal)

Abstract

Soil carbon modeling is an important tool to inform scientists, land managers, and policy makers about the impacts of land management decisions on soil health and climate change mitigation. Models can require a wide range of data inputs to make predictions, not all of which are readily available but can often be substituted with estimates. Understanding the impact that inputs have on the model output is critical to understand the uncertainties of their predictions. This study evaluated the output of the RothC soil carbon model using three potential evapotranspiration (PET) models (Tegos et al. 2017, Droogers and Allan 2002, and Thornthwaite and Mather 1955; Te, DA, and TM, respectively) to estimate open pan evaporation, and three vegetation indices (NDVI, SAVI, and MSAVI) from satellite imagery to estimate corn (*Zea mays* L.), soybean (*Glycine max* (L.) Merr.), and wheat (*Triticum aestivum* L.) yield to convert to C input for the RothC model to predict soil organic carbon over eleven years at a research farm in Michigan. The objectives of this study were to evaluate the correlation with observed data for each estimated input as well as the variability in RothC output they produced. The TM, Te, and DA PET models resulted in 13%, 38%, and 40% wet bias, respectively, resulting in increases of 1.6, 5.5 and 7.4 Mg C ha^{-1}, respectively, over the baseline model output. All three vegetation indices estimated corn yields poorly (R^2 = 0.25, 0.26, and 0.26 for NDVI, SAVI, and MSAVI, respectively), but soybean yields exceptionally well (all R^2 = 0.91). However, despite NDVI producing significantly higher values (p <

0.001), there were no significant differences between each index's estimated yield used to calculate C input for RothC, and the resulting model runs are almost indistinguishable.

Keywords

soil organic carbon; vegetation indices; model uncertainty

Abbreviations

DA, Droogers and Allen (2002) PET model; ESM, equivalent soil mass; KBS, Kellogg Biological Station; MSAVI, modified soil-adjusted vegetation index; NDVI, normalized vegetation index; NIR, near-infrared; OPE, open pan evaporation; P, total precipitation; PET, potential evapotranspiration; RS, remote sensing; SAVI, soil-adjusted vegetation index; T, air temperature; Te, Tegos et al. (2017) PET model; TM, Thornthwaite and Mather (1955) PET model; VI, vegetation index; Y, yield

1. Introduction

Soil organic matter (SOM) is a key soil health indicator which enhances many soil processes and ecosystem services, such as water infiltration and retention, aeration, nutrient cycling, and pollution remediation. SOM has long been understood to be highly sensitive to climate and land management practices (Jenny 1961, Tate et al. 1985). SOM content that has fallen below 2% by weight (equivalent to about 1% soil organic carbon (SOC)) can classify soil as unstable (Kemper and Koch 1966) and has been recognized as a threshold for crop productivity (Aune and Lal 1997).

Agricultural soil has also been identified as a potential medium for mitigating climate change (Lal 2004, 2016) through management practices which have been demonstrated to restore soil organic carbon lost through decades of tillage and erosion (Uri 2001, Lal et al. 2011, Roe et al. 2019). While the topic has been hotly debated over the past several years (Lal et al. 2015, Lugato et al. 2018, Baveye et al. 2020), scientists continue to investigate where SOC can be restored, how, and by how much (Chambers et al.

2016, Gautam et al. 2020), as well as to project the likely outcome of SOC content (Jones et al. 2005, Gottschalk et al. 2012, Maas et al., 2017, Gollany and Polumsky 2018, Gautam et al. 2022).

To aid the assessment of the land's potential to sequester carbon, a variety of modeling methods have been employed to estimate the effects of land management on soil carbon dynamics, such as biogeochemical process models and machine learning (Riggers et al. 2019, Gautam et al. 2022). The RothC model (Jenkinson 1990) is a widely-used biogeochemical process model to characterize and predict SOC from field-scale to global SOC stocks (Jones et al. 2005, Maas et al. 2017, Teixeira et al. 2021) and has been incorporated into at least one Earth System Model (Watanabe et al. 2011). It was developed specifically to model the turnover of SOC in topsoil.

Biogeochemical process models often require comprehensive input data including climate, plant characteristics and productivity, soil properties, and field management, observations for which are often unavailable. Predictive functions can supply missing data for a wide variety of climate and soil attributes. For example, open pan evaporation (OPE), a required input for the RothC soil carbon model (Jenkinson et al. 1990), is a climatological measurement used often by farmers and ranchers to plan irrigation applications. It is measured as the depth of water which evaporates from a cylindrical pan after 24 hours. Potential evapotranspiration (PET) is the maximum potential moisture that can be removed from the land surface through evaporation and plant transpiration, assuming water is not limiting. OPE can then be estimated with PET predictive models on a daily or monthly scale.

PET can be estimated from simple models using temperature alone (Thornthwaite and Mather 1955, Blaney and Criddle 1962)), models based on solar radiation (Priestley and Taylor 1972, Hargreaves 1975, Droogers and Allan 2002, Tegos et al. 2017), or "combined" models requiring an array of climate variables (Penman and Keen 1948, Monteith 1965, Van Bavel 1966). A range of environmental factors can serve as inputs to PET calculations, such as air temperature and humidity, precipitation, wind

velocity, and solar radiation. However, some of these factors are often difficult to obtain measurements for, particularly when point data at a specific locale are desired, requiring the use of a simpler model.

Remote sensing (RS) also has the potential to supply proxy data, such as determining if a field is bare or covered with vegetation, and if vegetated, how much biomass it contains or yield produced. This in turn can be used to estimate how much C in a system is added to the soil via roots and surface litter – a critical component of soil carbon models. Remote sensors collect their data as electromagnetic radiation as solar radiation reflects off various surfaces on land as well as in the atmosphere. The energy is segmented by wavelength and recorded in "bands", including ranges in the visible and infrared spectrums. Each band records a brightness value of its assigned wavelength range for each pixel in each image it records. The number of bands and range of wavelength in each band is called the spectral resolution of that sensor. The time period (hours, days, weeks) between images captured of the same scene on the ground is the temporal resolution. The dimensions on the ground which each pixel represents within each image is the spatial resolution.

Vegetation indices (VIs) are mathematical models constructed from one or more bands in a sensor. The Normalized Difference Vegetation Index (NDVI), Soil Adjusted Vegetation Index (SAVI; Huete 1988), and the Modified Soil Adjusted Vegetation Index (MSAVI; Qi et al. 1994a) are canopy reflectance models designed to numerically represent the greening or browning of vegetation. NDVI is one of the most widely-used indices to correlate directly with crop yield (Thenkabail et al. 1992, Zhu and Liu 2015, Georgi et al. 2018) as well as indirectly, such as estimating the leaf-area index (LAI), for LAI-based yield models (Baez-Gonzalez et al. 2005). NDVI is based on the inverse relationship between the red and near-infrared (NIR) wavelength reflectance of vegetation.

NDVI can be sensitive to background influences, such as bare soil and residue cover (Jones et al. 2015), which introduces limitation and uncertainty. Soil reflectance when soil is dry is higher than leaf

reflectance (Goel 1988). Hence, SAVI was developed to minimize the effects of exposed soil through the plant canopy, a lesser issue during peak vegetative growth when the canopy is closed. A closer correlation was demonstrated with SAVI than NDVI for wheat yield (Liaqat et al., 2017). MSAVI was developed to reduce the soil brightness effect of SAVI while restoring some of the vegetation sensitivity lost by it. Yang and Everitt (2012) found MSAVI to have a higher correlation with grain sorghum yield than either NDVI or SAVI. Atmospheric scattering of solar rays as well as solar and viewing geometry (angle of the sun or sensor) can impact all these indices.

There are many uncertainties inherent in modeling, regardless of the tool or context. In modeling, uncertainty and uncertainty analysis are broad terms encompassing a number of different methods to address system knowledge gaps and measurement errors (Larocque et al. 2008a, Larocque et al. 2008b, Asseng et al. 2013, Roux et al. 2014, Wang and Chen 2012). Uncertainties can be introduced through model inputs, parameters, structure, and the study scale, with substantial consequences to model output (Todd-Brown et al. 2013). For example, Todd-Brown et al. (2018) found that soil could be either a carbon source or sink depending on the method of soil temperature sensitivity employed.

With a growing interest by many individuals, organizations, and governments to implement carbon farming and other carbon-sequestration and -reduction initiatives (Chambers et al. 2016, Sharma et al. 2021, The White House 2021), it is more important than ever to identify sources of uncertainty in soil carbon models and reduce them as well as demonstrate methods to enhance their usability. This study analyzed uncertainty in the RothC model output for two alternative input sources (PET models and remote sensing yield estimates) through what Dale et al. (2017) termed a “within model” ensemble, using eleven years of agricultural data (1989 to 1999) in Michigan to validate SOC and corn (*Zea mays* L.), soybean (*Glycine max* (L.) Merr.), and wheat (*Triticum aestivum* L.) yield.

Prior studies have compared the relative accuracy of PET models to each other (de Jong and Tugwood 1987, Lu et al. 2005) and utilized individual PET models to estimate OPE for use in RothC (Guo et al. 2007, Todorovic et al. 2010, Yokozawa et al. 2010), but studies which compare RothC results with multiple alternative PET methods, demonstrating its sensitivity to them, appear to be lacking. This study included a comparison of three PET models – two radiation-based models (Tegos et al. 2017; Droogers and Allan, 2002) and one well-known temperature-based model (Thorthwaite and Mather, 1955) with two objectives: 1) to determine which of the three PET models (after conversion to OPE) provides the closest approximation to measured OPE and 2) to describe the RothC model's response to each. It was hypothesized that 1) the more complex radiation-based PET models would perform better against observations and 2) PET models with higher levels of evapotranspiration would result in higher SOC content reported by RothC, all else being equal.

Studies have also demonstrated the utility of RS to estimate total aboveground biomass or yield both independently and via coupling to crop growth models (Tucker 1980, Marshall et al. 2018, Awad 2019, Ines et al. 2013, Chao et al. 2019). RothC has been used to compare its estimated plant litter inputs to estimated inputs generated with the MODIS satellite (Hashimoto et al. 2011), but to date there is a dearth of studies which use RS data for input specifically to RothC for modeling soil carbon. This study will therefore also include a comparison of three common VIs – NDVI, SAVI, and MSAVI – to determine their effectiveness in supplying yield data for conversion to C input to RothC for three additional objectives: 1) to determine the correlation between VI values and crop yield, 2) to compare C input calculated from VI-estimated yield to C input calculated from field measurements, and 3) to analyze the differences of each VI model's C input on the RothC model's output. It was hypothesized that 1) there would be a moderate but acceptable correlation (R^2 >= 0.50) between VIs and yield, 2) there would be no significant difference between SOC estimated from C inputs provided by VIs as from field

138 measurements, and 3) there would be little difference between RothC outputs using C input calculated
139 from VIs vs. field measurements.

140 2. Materials and Methods

141 2.1 Site

142 The Kellogg Biological Station (KBS) Long-term Ecological Research Program, located in Kalamazoo
143 County, MI (42.410, -85.372, elevation 288 m), has been run by Michigan State University since 1987.
144 Plots are approximately 1 ha in size and include treatments of corn, soybean, and wheat rotations.

145 The soil is classified as Kalamazoo fine-loamy, mixed mesic Typic Hapludalfs (43/38/19% sand/silt/clay
146 content) to a 30 cm depth, with a 5.5 pH (Crum and Collins 1995). The historical ecosystem in the region
147 was a mixture of hardwood forest, savannah, and prairie (Comer et al. 1995). The site was believed to
148 have been first tilled in 1850 to grow cereal crops, most likely wheat, corn, and oats, with corn and
149 soybeans dominating from 1954 onward (Tomecek and Robertson 1996).

150 Six no-tillage plots, which began the eleven-year experimental period (1989-1999) as a two-year corn-
151 soybean rotation and then converted to a three-year corn-soybean-wheat rotation in 1995 (see
152 Supplementary Table S1), were selected for this study together with four natural grass never-tilled
153 control plots.

154 2.2 RothC Model

155 RothC, standard version 26.3, runs on a monthly timestep due both to the nature of SOC to change
156 slowly over time and the exclusion of nitrogen dynamics which would require a smaller timestep
157 (Jenkinson 1990). It begins with a 10,000-year spin-up period, during which it evolves soil to a point
158 where carbon content is at equilibrium at a level compatible with what would have been natural,
159 undisturbed soil at the site. Next, an historical period is run starting at the point the land was converted

160 to farming from its natural state, using best-estimate data from assumed crops and their calculated
161 levels of carbon input. Then the model is run through an experimental period and, optionally, into the
162 future.

163 The RothC User's Guide (Coleman and Jenkinson 2014) provides in-depth details of the calculations of
164 the model and are summarized here. The model requires monthly plant-based C input to be supplied,
165 which is split between four active SOM-decomposition compartments and a small amount of inert
166 organic matter (an inactive pool where SOM is not decomposed and permanently stored). The active
167 pools are Decomposable Plant Material, Microbial Biomass, Resistant Plant Material, and Humified
168 Organic Matter, listed in order of their rate of decomposition, from fastest to slowest.

169 Each pool processes SOM decomposition with its own rate constant in a first-order decay process and
170 modified by additional climate and soil cover factors. Monthly average air temperature is used to
171 calculate a rate-modifying factor value which rises exponentially from -10 °C until about 10 °C, indicating
172 an exponentially increasing rate of decomposition while soil is cold. Above 10 °C, the factor value rises
173 approximately linearly with increasing temperature. A topsoil moisture deficit is calculated from total
174 monthly precipitation, total OPE, clay content, and a monthly soil cover indicator (bare vs. not bare).
175 Evaporation in bare soil (no growing plants) occurs at a reduced rate, slowing the drying of soil. The
176 moisture rate-modifying factor value is then calculated as a function of the topsoil moisture deficit such
177 that decomposition is fastest when soil is moist and slowest when very dry:

178 $$PET_{rothc} = 0.75(OPE) \quad (1a)$$

179 where PET_{rothc} (mm) is RothC's internal conversion of the OPE input data to PET. Each month's soil
180 moisture deficit (SMD, mm) is calculated as:

181 $$SMD = P - PET \quad (1b)$$

where P is total monthly precipitation (mm). The maximum total soil moisture deficit ($TSMD_{max}$) is a fixed value derived from the clay content:

$$TSMD_{max} = -(20.0 + 1.3(\%clay) - 0.01(\%clay)^2) \quad (1c)$$

If soil is bare, then $TSMD_{max}$ is divided by 1.8 to limit the loss of moisture from soil due to evapotranspiration.

The moisture rate-modifying factor is then calculated as:

$$b = 1, \text{ if } TSMD_{acc} < 0.444(TSMD_{max}) \quad (1d)$$

where $TSMD_{acc}$ is the running monthly accumulation of the TSMD, calculated as the sum of the current and prior month's SMD. Otherwise,

$$b = 0.2 + 1.1 * \frac{(TSMDmax - TSMDacc)}{(TSMDmax - 0.444TSMDmax)} \quad (1e)$$

The monthly soil cover indicator also triggers a toggle between two constant values (indicating soil is vegetated vs. soil is bare) as the final SOM pool decomposition rate-modifying factor value. It serves to slow SOM decomposition if plants are actively growing.

Clay content is also used to adjust the amount of C lost as CO_2 during decomposition. Soils high in clay content (around 30% clay) lose exponentially less C as CO_2, than soils with low clay. In high clay soils, more C is transferred from the Decomposable and Resistant Plant Matter pools (which are subject to high C loses as CO_2) to the Microbial Biomass and Humus pools (where C loss is much slower).

Soil depth in RothC version 26.3 is limited to topsoil only. It expects 23 cm, but actual depth can be supplied.

2.3 Statistical Analysis

All computer processing, including statistical analysis, was performed in R software (version 3.6.1, R Core Team 2019). Linear regressions were used to evaluate observed vs. calculated OPE and observed yield vs. VI values. Additionally, the coefficient of determination (R^2) and root mean squared error (RMSE) were calculated:

$$\text{RMSE} = \sqrt{\frac{\sum_{i=1}^{n}(O_i - P_i)^2}{n}} \quad (2)$$

where O_i is the *i*th observed value and P_i is the *i*th predicted value.

Temperature and P from the Detroit vs. Kalamazoo stations and C input calculated from VI-estimated vs. observed yield were evaluated with paired, two-sided Wilcox Signed-Rank t-tests.

The VIs were tested for significant differences between their means as well as the estimated yield calculated from linear regressions of the observed yield to each VI's value. One-way ANOVA was run with the *aov()* function and analyzed with *HSD.test()* (Tukey test) from the agricolae package (de Mendiburu 2021) to identify significant differences between VIs.

2.4 Historical Weather Data

Daily Summary data of temperature (T, minimum and maximum) in °C and P in mm were downloaded from the NOAA National Climatic Data Center (NCDC; Menne et al. 2012a, Menne et al. 2012b) from several weather stations close to the agricultural plots. Multiple MI stations were selected, with data coming preferentially from two Kalamazoo-area stations positioned two and 24 km from the KBS site, respectively (USC00203504, GULL LAKE BIOLOGICAL STATION, MI US; USW00094815, KALAMAZOO BATTLE CREEK INTERNATIONAL AIRPORT, MI US). Additional sites 20 to 50 km away, primarily to the southwest, supplied any remaining missing data. These were aggregated into monthly average T and total monthly P.

While T and P are almost universal measurements collected at weather stations in this network through time, OPE is much less common. The closest observations of OPE to the KBS site were at the "DETROIT CITY AIRPORT, MI US" station (USW00014822), approximately 170 km to the east. In order to determine if this was an acceptable source of OPE data, T and P data were correlated with the Gull Lake Biological Station data. Daily T correlated closely (R^2 = 0.94, RMSE = 2.7 °C), while P was correlated by month with R^2 values ranging from 0.26 to 0.63 (data not shown). However, T and P from the Detroit and Kalamazoo stations were statistically different ($p < 0.5$) with 13.5 mm greater mean monthly P in the Kalamazoo area than Detroit. This would result in substantially lower OPE measurements if the Detroit data were used as-is. Therefore, in lieu of actual observations in the Kalamazoo area, the PET model which demonstrated the closest fit to the Detroit data was used to estimate PET with Kalamazoo-area data, converted to OPE, and downscaled to address the wet bias. Then all PET models used for the study were converted to OPE but without downscaling to highlight the differences in RothC's response to them. For the remainder of this study, all references to "PET model output" include subsequent conversion to OPE.

The Thornthwaite and Mather (1955) PET model output was found to have the closest correlation to Detroit OPE measurements, though with a 21.7 mm mean monthly positive bias, or 13%. To address the bias of the model, each month was then reduced by 13%. This downscaled model was therefore used to serve as the proxy observations with the Kalamazoo-area climate data for the model scenarios in this study.

2.5 Open Pan Evaporation

Thornthwaite and Mather (1955) (TM)

This model only requires T measurements and calculates PET on a monthly basis. When mean T is less than 27 °C, then PET is defined as:

$$\text{PET (mm month}^{-1}) = 0.53 * \left(\frac{10*\text{Tm}}{\text{I}}\right)^{\text{a}} * \text{U} \quad \text{(3a)}$$

where Tm is the monthly mean T for a given month, U is a constant dependent on which the month of the year is being calculated, and a is a coefficient defined as:

$$a = (0.000000675*I^3) - (0.0000771*I^2) + (0.01792*I) + 0.49239 \quad (3b)$$

where I is the annual heat index defined as:

$$I = \sum_{j=1}^{12} i_j, \text{ and } i = (0.2 * T_j)^{1.514} \quad (3c)$$

When mean monthly temperatures are equal to or greater than 27 °C, then

$$PET = -0.015 * T^2 + 1.093 - 14.208 \quad (3d)$$

Droogers and Allen (2002) (DA)

Droogers and Allan (2002) modified Hargreaves and Samani (1985) to include P in the model:

$$PET = 0.0013 * ER * \left(\left(\frac{T_{min}+T_{max}}{2}\right) + 17\right) * (T_{max} - T_{min} - (0.0123 * P))^{0.76} \quad (4a)$$

where P is total daily precipitation (mm). ER is a water-equivalent calculation of extraterrestrial radiation (defined as solar radiation received at the top of Earth's atmosphere on a horizontal surface):

$$ER = 15.392 * d_r^2 * ((\omega_s * \sin(lat) * \sin(\delta)) + (\cos(lat) * \cos(\delta) * \sin(\omega_s))) \quad (4b)$$

where d_r is the distance between Earth and the sun, ω_s is the sunset hour angle, lat is the latitude in radians, and δ is the solar declination, each defined as follows:

$$d_r = 1 + 0.033 * \cos\left(\frac{2*\pi}{365} * J\right) \quad (4c)$$

$$\omega_s \text{ (rad)} = \arccos(-\tan(lat) * \tan(\delta)) \quad (4d)$$

$$\delta = 0.4093 * \sin\left(\frac{2*\pi}{365} * J - 1.405\right) \quad (4e)$$

$$lat = LDD * \left(\frac{\pi}{180}\right) \quad (4f)$$

where J is the Julian day of the year and LDD is latitude in decimal degrees.

Tegos et al. (2017) (Te)

Tegos et al. (2017) developed a new model through parametric modeling to derive a relatively simple radiation-based model:

$$PET = \frac{a' * R_a}{1 - c' (T_{min} + T_{max})/2} \quad (5)$$

where a' and c' are calibrated parameters and R_a is extraterrestrial radiation (kJ m^{-2}), defined as:

$$R_a = \left(\frac{24*60}{\pi}\right) 82 * d_r^2 * ((\omega_s * \sin(lat) * \sin(\delta)) + (\cos(lat) * \cos(\delta) * \sin(\omega_s))) \quad (5a)$$

OPE

PET is converted to OPE by:

$$OPE\ (mm) = PET/0.75 \quad (6)$$

To provide a more consistent comparison to the monthly TM model and to prepare the data for RothC input, the results from the daily DA and Te models were first aggregated by month then correlated to monthly observed OPE.

2.6 Remote Sensing Inputs

2.6.1 Landsat Satellite Imagery

Landsat satellites are launched and retired periodically by NASA. The Landsat 4 and 5 satellites began orbit in 1982 and 1984, respectively. Both have spatial resolution of 30 m per image pixel with a temporal resolution of 16 days. Scenes (images) were downloaded from the USGS Earth Explorer (USGS n.d.(a)). The VIs in this study were derived from Thematic Mapper on-board sensors (Masek et al. 2006) and produced on-demand through the USGS Earth Resources Observation and Science (EROS) Center's

Science Processing Architecture On Demand Interface (USGS 2017), and downloaded in NetCDF format. The data provided were corrected for atmospheric effects such as aerosol scattering and thin clouds.

The satellite data for this study includes some gaps in years when weather conditions did not permit the capture of suitable images (see Supplementary Table S1 and Section 2.6.3).

2.6.2 Vegetation Indices

Landsat satellites collect image data across seven spectral bands according to wavelength. The VIs used in this study combine values from the red and near infrared bands (Masek 2006, USGS n.d.(b)).

NDVI describes the greenness (density and health) of vegetation and is the ratio of the difference between the near infrared and red bands to their sum:

$$\text{NDVI} = \frac{\text{NIR}-\text{RED}}{\text{NIR} + \text{RED}} \quad (7)$$

where NIR is the near-infrared band and RED is the red band.

SAVI modifies NDVI to correct for the influence of soil brightness when vegetative cover is low (Huete 1988):

$$\text{SAVI} = (1 + \text{L}) * \frac{\text{NIR}-\text{RED}}{\text{NIR} + \text{RED} + \text{L}} \quad (8)$$

where L is a correction factor for the density of vegetation where 0 indicates high density and 1 indicates low density. When L is 0, equation 6 is identical to NDVI. The EROS on-demand system hard-codes L = 0.5.

MSAVI provides a self-adjusting L correction factor (Qi et al. 1994a, Qi et al. 1994b):

$$\text{MSAVI} = \frac{\left(2*\text{NIR}+1-\sqrt{((2*\text{NIR}+1)^2-8*(\text{NIR}-\text{R}))}\right)}{2} \quad (9)$$

Ecologically meaningful output values of each index range from 0 to 1.

2.6.3 Remote Sensing Yield Estimation

The yield estimated by RS (Y_{RS}) is given by:

$$Y_{RS} = m * VI + b \quad (10)$$

where m is the slope and b is the y-intercept of a linear regression relationship between the observed yield vs. VI.

Studies have demonstrated greater predictive power of RS yield estimation when multiple images throughout the growing season are used (Teal et al. 2006, Liu et al. 2010, Zhu and Liu 2015). However, due to a severe limitation of viable satellite images and a lack of agronomic data to verify crop growth stages, a single image captured as close to the estimated maximum wet biomass stage was used in this study.

No planting dates were available for the time period chosen, so they were estimated as May 15 and June 1 for corn and soybeans, respectively, based on later planting data from KBS. However, there is considerable variability in recorded planting dates with a 23- and 26-day range for corn and soybeans, respectively, from 2015 through 2019 from which the planting dates were estimated from. VIs are most effectively used when corresponding to growth stages of crops (Teal et al. 2006). Thenkabail et al. (1992) measured maximum wet biomass to be at about 100 and 80 days after planting corn and soybeans, respectively, which also roughly corresponds to the end of the blister (R2) and pod-filling stages (R6) when the silks begin to brown on corn and seeds have developed in soybean pods, respectively. Therefore, given the estimated planting dates, peak AGB – and NDVI readings – were expected to occur about the third and fourth week of August for soybeans and corn, respectively, so these were used as target dates to collect satellite images from. Actual dates of scenes available are recorded in Supplementary Table S1.

In those years without suitable satellite images, the observed yield was substituted for that year (soybean in 1990 and 1992, and wheat in 1995 and 1998). For all other years, the VI was used to estimate yield for that year, then C_I calculated from that estimate to use for RothC input.

This study utilized the Bolinder et al. (2007) method to calculate annual C input, considered one of the most accurate methods currently available (Keel et al., 2017):

$$C_I\ (g\ C\ m^{-2}\ yr^{-1}) = [C_P * S_P] + [C_S * S_S] + [C_R * S_R] + [C_E * S_E] \quad (11)$$

where C_I is the annual C input to soil, C_P is the total C from the harvested plant parts (such as grains or beans), C_S is the remaining above-ground plant parts (stover), C_R is C from roots, C_E is extra-root C (such as from root exudates), and the S variables are the proportions of each C source that are returned to the soil. For example, after a corn harvest where 70% of the plant residue is also removed from field, $S_P = 0$ (no grain left on the field), $S_S = 0.3$ (30% stover left on the field), $S_R = 1$ (all roots remain), and $S_E = 1$ (all root exudates remain).

C_P was calculated by multiplying the dry harvest yield mass by 0.45 to obtain the C content of the grains

Crop	Crop Parameter	Value	References
Corn	lbs bu^{-1} conversion factor	56	https://grains.org/markets-tools-data/tools/converting-grain-units/
Corn	Grain moisture content	12.9%	Martin and Leonard (1949)
Corn	Harvest Index	0.48-0.54*	Sinclair (1998), Prince et al. (2001)
Corn	Shoot:root ratio	4.15	Prince et al. (2001), Bolinder et al. (2007)
Soybeans	lbs bu^{-1} conversion factor	60	https://grains.org/markets-tools-data/tools/converting-grain-units/
Soybeans	Grain moisture content	8%	Martin and Leonard (1949)
Soybeans	Harvest Index	0.34-0.40*	Balboa et al. (2018)
Soybeans	Shoot:root ratio	5.2	Prince et al. (2001), Bolinder et al. (2007)
Wheat	lbs bu^{-1} conversion factor	60	https://grains.org/markets-tools-data/tools/converting-grain-units/
Wheat	Grain moisture content	10.6%	Martin and Leonard (1949)
Wheat	Harvest Index	0.37-0.47*	Austin et al. (1980), Sinclair (1998), Prince et al. (2001)
Wheat	Shoot:root ratio	6	Prince et al. (2001)

Table 1. MI site crop parameters for calculating annual C input (Bolinder et al. 2007) for the RothC model

* Harvest Index values for some crops have reportedly increased over time. The trend of values reported in the literature for soybeans were statistically modeled over time and estimated values used.

(Bolinder et al. 2007).

2.7 Modeling Run Setup

The reference site for soil organic matter studies at the KBS is a mown grassland which has never been tilled nor in agriculture (KBS n.d.). This site supplied the initial SOC content and crop parameter value for the equilibrium spin-up period. The crop parameter is the decomposable:resistant plant material ratio of the predominant vegetation, which was 0.67 for grasslands (Coleman et al. 1997). Farming is assumed to have begun in 1850 with a 2-year corn-wheat rotation. Historical yields from 1850 were obtained or estimated from county-level census data for Kalamazoo County, MI (USDA-NASS 2019). Additional crop parameters were derived from the literature (Table 1).

Total organic C stock (TOC) at equilibrium was calculated to a fixed depth (TOC_{FD}) by averaging the surface (to 25 cm) OC percentages of four control plot replicates over all available years (1989-2001), averaging the bulk densities measured over the same time and depth, then calculating the C content as follows:

$$TOC_{FD} = D * BD_C * OC_C\% \quad (12)$$

where D is a constant of 25 cm, and BD_C and OC_C% are the mean bulk density (soil weight per volume) and the mean OC percentage, respectively, from the control plots. This resulted in an initial TOC_{FD} content of 59.8 Mg C ha^{-1}. The C_I for the spin-up period was then calculated by RothC in reverse mode (Coleman et al. 1997), where the model is given the SOC content and it calculates the C_I required to produce it.

The treatment plot soil had higher bulk density than the control plots, due to years of tillage breaking down the structure of the soil and compaction from heavy farm equipment, which can lead to artificially inflated C content values (Ellert and Bettany 1995). Therefore, the TOC was calculated on an equivalent

362 soil mass basis (TOC_{ESM}; Lee et al. 2009) by substituting the mean control plot bulk density in Equation
363 12 for all treatment replicates:

364 $$TOC_{ESM\text{-}Yx} = D * BD_C * OC_T\%_{Yx} \quad (13)$$

365 where Yx is each year sampled, BD_C is the mean bulk density from the control plots, and $OC_T\%_{Yx}$ is the
366 annual mean OC percentage for all treatment plot replicates. Calculating TOC on an equivalent soil mass
367 basis resulted in a mean reduction of TOC of 13.5 Mg C ha^{-1} over TOC calculated on a fixed-depth basis
368 (Supplementary Figure S2). The $TOC_{ESM\text{-}Yx}$ values were then used as the observed SOC content at the site

Model Run	Model Description	OPE Source	C Input Source
1	Observational Baseline	Observed*	Observed**
2	PET Estimate-TM	Thornthwaite and Mather (1955)	Observed**
3	PET Estimate-DA	Droogers and Allan (2002)	Observed**
4	PET Estimate-Te	Tegos et al. (2017)	Observed**
5	RS Yield Estimate-NDVI	Observed*	NDVI
6	RS Yield Estimate-SAVI	Observed*	SAVI
7	RS Yield Estimate-MSAVI	Observed*	MSAVI

Table 2. RothC model run descriptions.

* Observed open pan evaporation (OPE) is actually calculated from Thornthwaite and Mather (1955) with Kalamazoo weather data and bias-corrected .
** Observed C input is derived from harvested yields and converted via Bolinder et al. (2007).

369 for the experimental period.

370 The RothC baseline model run with observational data was calibrated to the observed TOC_{ESM} through
371 "inverse modeling" (repeatedly running the model with adjusted C_I values until model TOC output
372 matches observed TOC (Coleman et al. 1997)). Additional RothC model runs were then constructed with
373 PET model output to test their effect in place of the observed OPE, as well as runs with C_I calculated
374 from RS-based yield estimates from VIs (Table 2).

In this study as a whole, the certainty of the "control" RothC model run, which is ideally constructed entirely from observations, is of lesser importance than the "treatment" model runs constructed from alternative inputs (OPE or C_I). Since only one model input was substituted at a time and all else held equal, the primary focus was on the differences each alternative input (PET- or VI-estimated values) had on the output. That said, the control was constructed as carefully as possible to reasonably meet the ground truth TOC levels for a reliable base of comparison.

3. Results

3.1 Potential Evapotranspiration Estimators

PET model output was evaluated for goodness of fit to measured OPE from the Detroit-based weather station data (Figure 1 a-c). There was a noticeable difference between radiation-based and T-based models, with biases of 40.4%, 37.7%, and 13% for DA, Te, and TM, respectively. TM had the highest R^2, lowest RMSE, slope closest to 1 (1.05), and least bias. After correcting for bias, the RMSE of the TM

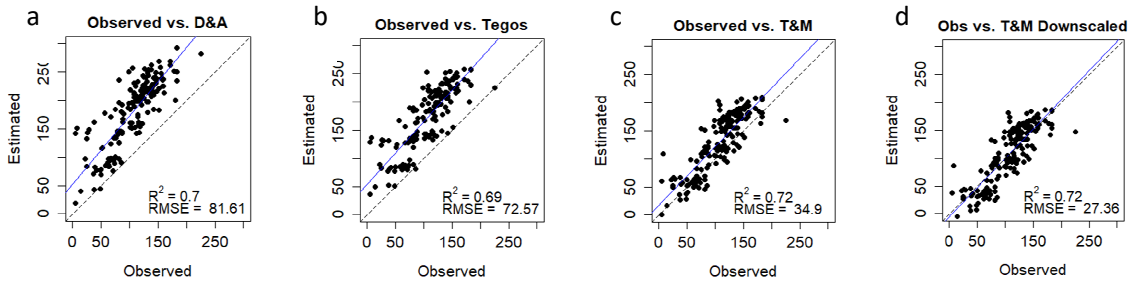

Figure 1. Potential evapotranspiration model correlations after conversion to open pan evaporation (mm month^{-1}). Graphs a through c are raw correlation with Detroit-area climate data. Graph d is the Thornthwaite and Mather (T&M; 1955) result after bias correction. D&A=Droogers and Allen (2002), Tegos=Tegos et al. (2017).

model was reduced 22% and was 66% and 62% lower than DA and Te, respectively.

Figure 2 presents the differences in RothC results with each PET model output replacing the observed OPE (TM bias-corrected, Figure 1d) with all else being equal, including C input (Runs 1 through 4, Tables

2 and 3). Reflecting each model's bias, each result displays a substantial difference in final TOC_{ESM} (Table 3). RothC Observed and RothC DM OPE model output by 1999 represent a difference of 7.4 Mg C ha^{-1}. Figure 2 illustrates a compounding increase over time, averaged at 0.2 Mg C ha^{-1} yr^{-1} in this study.

A quadratic relationship was noted between the % wet bias and resulting % change in TOC_{ESM} in RothC results by 1999 among the PET models (Supplementary Figure S1).

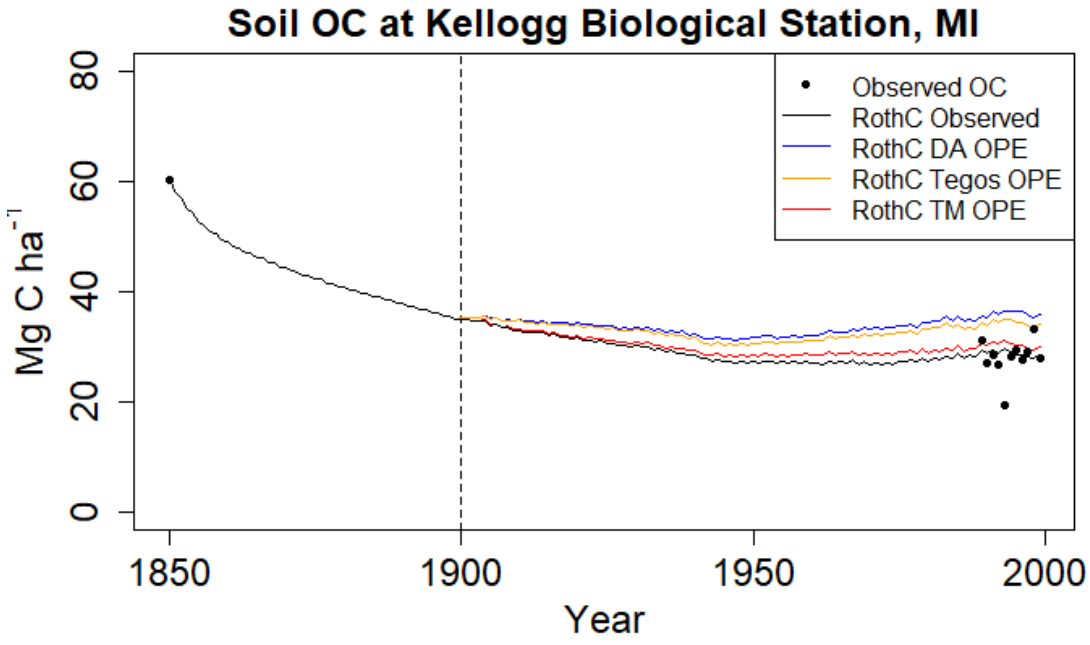

Figure 2. RothC model run results with three potential evapotranspiration models, converted to open pan evaporation (OPE) and a baseline run using observed OPE (which is downscaled TM in this study). Dashed vertical line denotes the beginning of the experimental period for the OPE comparison. DA=Droogers and Allen (2002), Tegos=Tegos et al. (2017), TM= Thornthwaite and Mather (1955).

		1999 TOC_{ESM} Stocks		1999 SOC %		
Model Run	Model Description	Mg C ha^{-1}	Δ from Baseline	%	Δ from Baseline	% Δ from Baseline
1	Observational Baseline	28.4	--	0.95	--	--
2	OPE Estimate (DA)	35.8	7.4	1.19	0.24	20
3	OPE Estimate (Te)	34.0	5.5	1.13	0.18	16
4	OPE Estimate (TM)	30.0	1.6	1.00	0.05	5
5	NDVI Yield Estimate	29.0	0.6	0.97	0.02	2
6	SAVI Yield Estimate	28.9	0.5	0.96	0.01	1
7	MSAVI Yield Estimate	28.8	0.4	0.96	0.01	1

Table 3. RothC model run results in total organic carbon calculated on an equivalent mass basis (TOC_{ESM}) and as % SOC for model runs with three different open pan evaporation (OPE) model estimates and vegetation indices (VI). All TOC_{ESM} units are in Mg C ha^{-1}.

3.2 Remote Sensing Yield Estimators

NDVI values were generally lower for corn than soybeans (Table 4). Correlations were low for corn (R^2 =

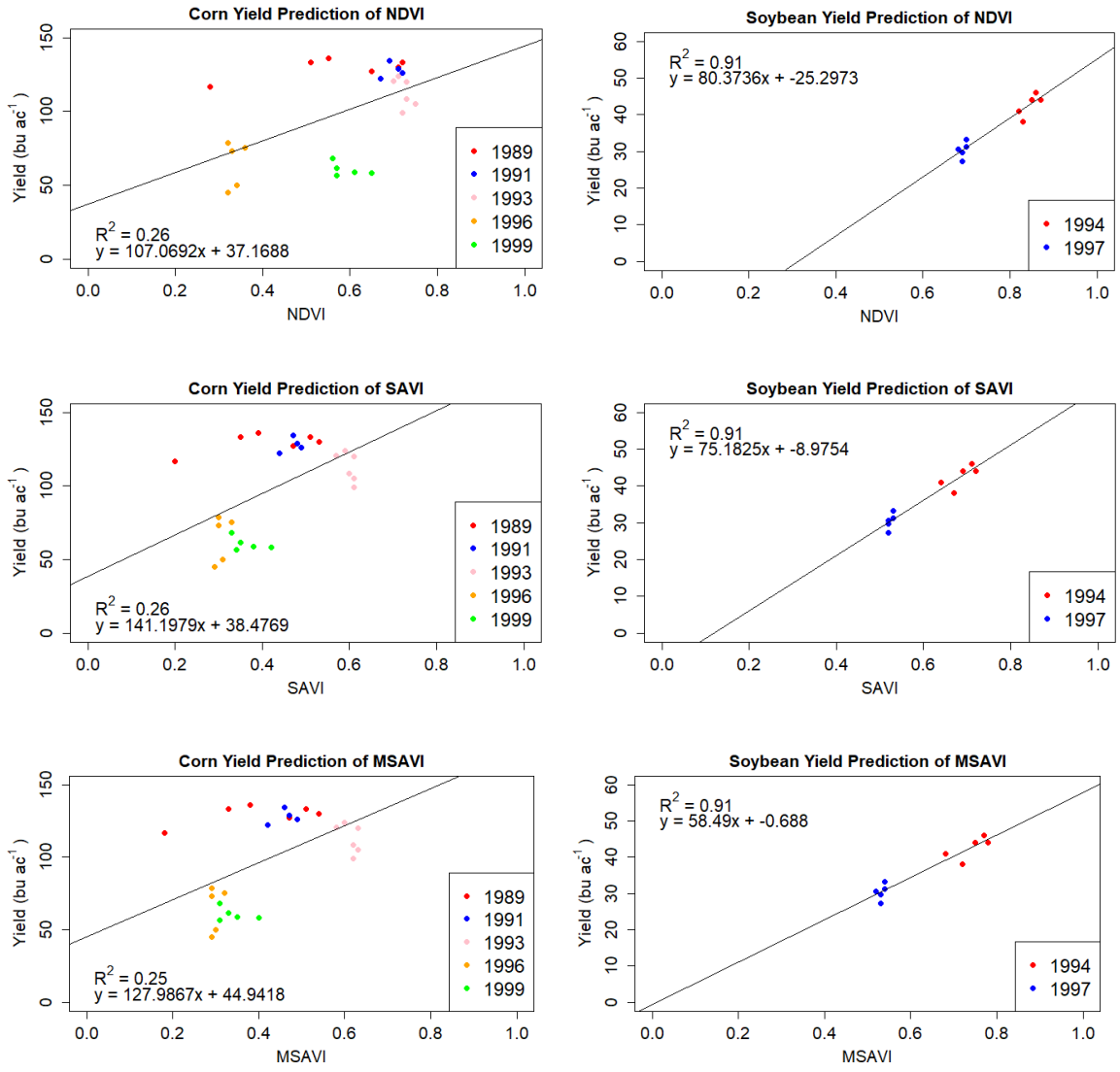

Figure 4. Scatterplots with linear equations between observed corn and soybean yield for each vegetation index. Different colored dots indicate different years' data.

0.25 to 0.26), and very high for soybeans (R^2 = 0.91), with SAVI the highest in each case (Figure 4).

Figure 4 shows that SAVI and MSAVI both substantially reduced the horizontal between-year variability over NDVI, as well as some horizontal within-year variability in corn, but not soybean. ANOVA analysis showed that NDVI values for both corn and soybeans were significantly ($p < 0.001$) higher than both SAVI and MSAVI (Supplemental Figure S3, Table 4). However, there were no statistical differences between the yield estimated by the linear regressions in Figure 4.

Three more RothC runs were constructed using the estimated values of yield for each vegetation index as the C input for the years 1989-1999, all else being equal and using the downscaled TM model as observed OPE input (Table 2). Although there are substantial differences between estimated yield and actual yield in some cases (Table 4), this still resulted in almost identical model runs (Figure 5, Table 3). By the end of the 11-year period, no index estimated a net difference in yields greater than 0.3 Mg ha^{-1}, and mean differences by crop type within each VI are nearly zero (Table 4). When converted to C_I, no single yield estimate from any index resulted in an absolute difference from C_i based on observed yield greater than 0.93 Mg C ha^{-1}, and most differences were less than 0.5 Mg C ha^{-1} (Supplementary Table

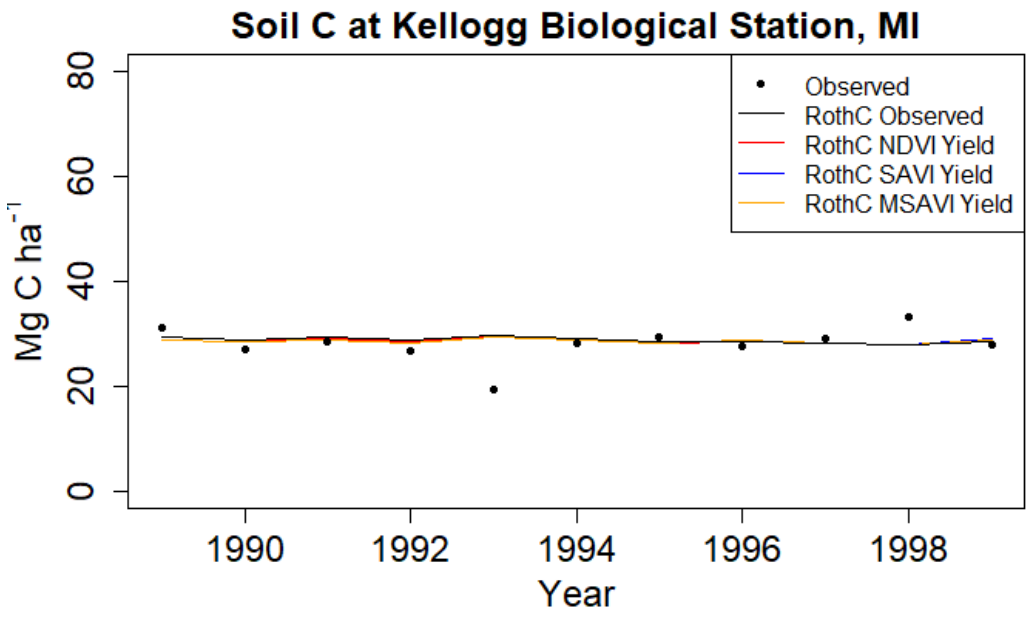

Figure 5. RothC model run results for multiple vegetation indices' yield estimates, converted to C input. NDVI=Normalized Difference Vegetation Index, SAVI=Soil Adjusted Vegetation Index, MSAVI=Modified Soil Adjusted Vegetation Index.

411 S2).

412

Index	Year	Crop	VI Value Mean	VI Value SE	VI n	Observed Yield Mean Mg ha^{-1}	Observed Yield SE Mg ha^{-1}	Yield n	VI-Estimated Yield Mg ha^{-1}	Observed-VI Estimated Yield Diff Mg ha^{-1}	Net Diff Mg ha^{-1}	Mean Diff by Crop Type Mg ha^{-1}
NDVI***	1989	Corn	0.58	0.16	45	8.14	0.44	6	6.24	1.89		
	1991	Corn	0.71	0.04	35	8.05	0.33	6	7.12	0.93		Corn:
	1993	Corn	0.72	0.02	45	7.11	0.63	6	7.19	-0.08		-0.07
	1994	Soybeans	0.84	0.03	40	2.68	0.2	5	2.66	0.02		
	1996	Corn	0.34	0.02	42	4.05	0.99	5	4.63	-0.57		Soybeans:
	1997	Soybeans	0.69	0.02	45	1.91	0.14	5	1.90	0.02		0.02
	1999	Corn	0.59	0.05	45	3.82	0.29	5	6.31	-2.50	-0.29	
SAVI	1989	Corn	0.42	0.12	45	8.14	0.44	6	6.15	1.99		
	1991	Corn	0.49	0.04	35	8.05	0.33	6	6.77	1.28		Corn:
	1993	Corn	0.59	0.02	45	7.11	0.63	6	7.66	-0.55		-0.06
	1994	Soybeans	0.68	0.05	40	2.68	0.2	5	2.65	0.03		
	1996	Corn	0.31	0.01	42	4.05	0.99	5	5.17	-1.12		Soybeans:
	1997	Soybeans	0.53	0.02	45	1.91	0.14	5	1.94	-0.03		0.00
	1999	Corn	0.37	0.04	45	3.82	0.29	5	5.71	-1.89	-0.29	
MSAVI	1989	Corn	0.41	0.13	45	8.14	0.44	6	6.13	2.01		
	1991	Corn	0.48	0.05	35	8.05	0.33	6	6.69	1.36		Corn:
	1993	Corn	0.61	0.02	45	7.11	0.63	6	7.74	-0.63		-0.04
	1994	Soybeans	0.73	0.06	40	2.68	0.2	5	2.64	0.04		
	1996	Corn	0.3	0.01	42	4.05	0.99	5	5.24	-1.19		Soybeans:
	1997	Soybeans	0.53	0.03	45	1.91	0.14	5	1.91	0.01		0.03
	1999	Corn	0.34	0.04	45	3.82	0.29	5	5.56	-1.75	-0.15	

Table 4. Summary of vegetation index values, observed yields, yields estimated from each vegetation index, and the difference between observed and estimated yield for each year indices were available. The Net Difference column is the sum of the differences over all years for each index and describes the final, net difference in yield carbon input to the soil by the end of the simulation for each index.

***Means of NDVI VI values (only) are significantly ($p < 0.001$) higher than both SAVI and MSAVI. There are no significant differences of estimated yield between the VIs.

4. Discussion

4.1 Potential Evapotranspiration Estimators

The difference in TOC_{ESM} by 1999 between PET-estimated model runs represents a 7.4 Mg C ha^{-1}, or 0.24%, difference in TOC_{ESM} between the baseline model and DA (Model Runs 1 and 2 in Table 3, respectively), and also represents a SOC % difference of 0.7%, which sounds inconsequential. The average SOC % in the upper 30 cm of topsoil in US mineral soil croplands (the most common soil type in mid-latitude agriculture) is 1.75% (West et al. 2013). About 1% SOC is considered by some as a threshold for minimally-required SOC to support agriculture (Moreno et al. 2006). Also, Figure 2 illustrates a compounding difference over time, averaged at 0.2 Mg C ha^{-1} yr^{-1} (or 0.02% SOC) in this study. If the simulations had continued for another 100 years under similar conditions, the difference in TOC_{ESM} would have been 14.8 Mg C ha^{-1}, or 1.4% SOC. Therefore, the difference indicated between the observed TOC_{ESM} and highest-modeled TOC_{ESM} in this study could in some cases indicate a difference between degraded and productive soil (Kemper and Koch 1966, Aune and Lal 1997). This also has important implications when results are being used to guide conservation efforts or other management decisions, such as those to identify degraded agricultural land for the purpose of restoration and carbon farming (Gautam et al. 2020), or efforts to implement the "4 per Thousand" initiative to increase SOC in managed soils by an average annual increase of 0.4% (Chambers et al. 2016).

Carvalhais et al. (2008) warned that the common feature of equilibrium spin-up in biogeochemical modeling can decrease model efficiency by introducing bias into the parameters. Wutzler and Reichstein (2007) argued that soils are, in fact, never in equilibrium; rather, older, undisturbed soils still accumulate C in the slowest pools, therefore, the decay rate for this pool is too high. In the case of RothC, this would be compensated by an overestimation of the C input. However, this concern would not affect the results of this particular study as the C input was equal in all scenarios, and because the topsoil deficit and

moisture rate-modifying factor calculations in RothC are not dependent on any plant attributes (Eq. 1a – 1e). Indeed, RothC has been noted to exhibit less bias than other agroecosystem models (Ranatunga et al. 2001), likely due in part to its relative simplicity with fewer parameters, each of which can introduce bias and uncertainty. However, Eq. 1a-1e do highlight the central role of PET on the effect of moisture to adjust the rate of decomposition.

Other biogeochemical models used in agriculture have built-in PET functions with two choices: limited data (T and P only) or robust data input (add radiation, wind speed, humidity, etc.). RothC's design is both a strength and weakness: actual observations can be provided, removing substantial bias and uncertainty due to the PET model employed, or a reliable PET method can be chosen. However, given the differences in bias among PET models in different climates (Guo et al. 2017), larger geographical studies with practical limits on their validation can influence results.

TM is the oldest and simplest model of those included in this study. Others who have compared multiple types of PET models – including T-only, radiation-based, and combination models – have noted increasing correlations with increasing complexity of models when full data was available for each equation considered (Amatya et al. 1995, Sentelhas et al. 2010). However, Bormann (2011) also demonstrated that 18 PET models of multiple types showed different sensitivities to climate trends with no common sensitivities between types of models. Sentelhas et al. (2010) demonstrated that simpler models such as Thornthwaite (1948) and Hargreaves and Samani (1985) are more reliable when only limited data are available, as was the case in this study.

4.2 Remote Sensing Yield Estimators

Despite low VI correlation with corn yield, the RothC model runs with VI-estimated C_i were almost indistinguishable. Although RothC is a relatively agile model sensitive to C input, there appeared to be a balancing effect related to the multiple crops in rotation; poorly-correlated corn rotated with well-

460 correlated soybean and later rotated with wheat which required observed data (for two years), along
461 with two of soybean years, due to the lack of acceptable satellite images available in a total of four years
462 (Supplementary Table S1). Another contributor to the smoothing effect was the alternating positive and
463 negative VI yield estimates over time (Figure 4 and Table 4). Even though corn had the lowest VI
464 correlation with yield, the mean NDVI C_i calculated over five years vs. observations were 2.398 and 2.38
465 Mg C ha^{-1}, respectively. Given the nearly identical C_i – calculated from yield estimates by a simple linear
466 model – it was no surprise that there were almost no differences between the resulting TOC_{ESM} modeled
467 using each. Despite high variability in VI values, this regression technique itself contributed to smoothing
468 the "noise" by basing all the yield estimates on the average through time, resulting in much less volatile
469 yield values (Supplementary Figure S3).

470 SAVI performed better than NDVI at yield estimation (Table 4), though at a very minor scale and with no
471 statistical significance, in agreement with Liaqat et al. (2017). SAVI was designed to be calibrated to soil
472 cover conditions with its L parameter, which ideally would vary with vegetation density (Huete 1988).
473 This implies knowledge of field conditions which negates some of the convenience of RS use. Also, the
474 EROS product holds the L value to a constant of 0.5, which is the most common use of SAVI and
475 recommended for a broad range of vegetation scenarios (Huete 1988), though Rondeaux et al. (1996)
476 found 0.16 to be the optimized value over a range of canopy covers as values of L = 0.50 resulted in a
477 higher standard deviation. Since the images used in this study were all assumed to be at or near peak
478 vegetative cover, SAVI may have been better calibrated to field conditions with a lower L value closer to
479 0.25 (Huete 1988), but as L approaches 0, SAVI equates to NDVI. Therefore, it is expected that the
480 greatest benefit of SAVI would be in lower vegetation density conditions.

481 Although MSAVI was expected to produce the closest correlation (R^2) to yield (Yang and Everitt 2012), in
482 this case there was almost no difference (Figure 4), although it did result in the least net difference
483 between observed and estimated yield (Table 4). In correcting for soil surface brightness, MSAVI

484 sacrifices some overall sensitivity to vegetation signals. This may be disadvantageous when vegetation is
485 at peak density and soil cover.

486 Lower VI values for corn than soybeans (Table 4) agree with Thenkabail et al. (1992). One possible
487 reason for the difference between them may be due to five years' worth of data used for corn at
488 uncertain growth stages, while there were only two years' worth for soybeans. It is possible that the
489 images used for soybean estimates were closer to their peak growth stages than for corn, though
490 without planting dates this could not be confirmed. However, even within same-year estimates (based
491 on multiple replicates of the same crop), there appears to be more variability in yield and VI estimates
492 for corn than soybeans.

493 There are four contexts of this variability within each individual panel in Figure 4: VI value (horizontal),
494 and yield value (vertical) differences either within the same year or between different years. Regarding
495 between-year horizontal variability of VI values, low VI values indicate smaller differences between the
496 red and NIR band values. This can occur during low photosynthetic activity or low NIR light reflectance,
497 such as from standing water or shadows. Holben (1986) suggested a solar zenith angle limit of 80° for
498 any pixel in order to limit shadows, which can lower VI values. Solar zenith angles for each scene used
499 ranged from 38.5° to 41.7° for corn and were 35.5° and 39.3° for soybeans, offering no apparent
500 explanation for the VI variability in between-year values for similar yields. The viewing geometry (angle
501 of the satellite sensor to the ground) can increase VIs with large off-nadir (not perpendicular to the
502 ground) viewing angles (Qi et al. 1994b). However, Landsat imagery has very small viewing angles, and
503 they are all the same for each image in this study. Horizontal between-year variability could also be
504 caused by images taken at different crop growth stages, with lower VI values due either to an under-
505 developed canopy or a crop entering senescence (drying in the field). Others have demonstrated
506 increased VI prediction accuracy when combined with crop growth stages (Bolton and Friedl 2013,
507 Maresma et al. 2020, Panek et al. 2020). Maresma et al. (2020) determined that V12 to R2 were the best

stages for most accurate prediction of corn yield, when corn reproductive parts (tassels and silks) have grown but not yet dried, though crop growth stages were not available for this study. They also found results were affected by time of day, with best results mid-morning and at 5:00 pm and avoiding 1:00 to 3:00 pm. All Landsat scenes in this study were taken between 3:39 and 3:59 pm (Supplementary Table S1).

Regarding within-year horizontal variability of VI values, standing water or wet soil in some plots, but not others, also has the potential to explain some of this variability, particularly if the satellite image was taken before the full canopy had developed. Wet soil results in higher NDVI values (Qi et al. 1994a) while standing water absorbs infrared wavelengths, which lowers NDVI (Sun et al. 2011). Weather data for the site indicate that the image in 1989, when there is particularly large horizontal (VI) but little vertical (yield) variability, was captured on the fourth day after the last rainfall, so particularly wet surface soil on this day is unlikely, and there had only been about 2.5 cm of rain over the week prior to that. Ponding is also less likely on higher-sand soils such as this site.

Regarding between-year vertical variability of yield values, where there is a range of yields for similar VI values, this could also be explained by a combination of images taken at different (and unknown) crop growth stages (Bolton and Friedl 2013, Maresma et al. 2020, Panek et al. 2020) combined with possible (and also unknown) differing statuses of crop health (Wang et al. 2016).

Regarding within-year vertical variability of yield values, this could be due to the limited range of pixels utilized for each plot, which are roughly centered on each plot so that the information closer to the edges is not included in the analysis. If there are pest, disease, or nutrient-related issues affecting the edges more than the center (including deer browse), the evidence for lower yields (lighter-colored leaves) could be excluded and the VI value would be artificially inflated relative to the yield for that plot.

Other methods have been used to achieve higher correlations with yield using NDVI as a basis. Maas (1988) achieved simulated sorghum yields within 2% of observations using NDVI and other satellite-based observations provided to a custom crop growth model. Baez-Gonzalez et al. (2005) found a prediction error of 9.2% in corn yield after using NDVI to predict LAI, then using an LAI-based model to predict yield. However, it is clear that the method of yield estimation is not required to be of highest quality in order to produce very acceptable RothC results.

Considering the unknowns (plant dates and growth stages) in this study, results may have benefitted from the application of RS techniques which aim to estimate crop growth stages (Sakamoto et al. 2005, Zhao et al. 2009, Liao et al. 2019). This could then be correlated to a VI curve to estimate yield (Quarmby et al. 1993).

5. Conclusions

This study identified limitation and potential in utilizing proxy inputs for observed OPE and C input to the RothC model for soil carbon stock estimation. A counterintuitive result, though with corroborating literature, suggests that PET models should be selected for simplicity when data are limited. In this study, the simplest model – Thornthwaite and Mather (1955) – proved the closest match and downscaled well to provide a proxy observation set. RothC is very sensitive to moisture changes and therefore wet bias in PET models, which produced correspondingly-elevated TOC results here in a perfect quadratic relationship with notable differences between model runs. The method of PET calculation used with biogeochemical models therefore has implications for their use in future projections of carbon stocks, particularly in croplands and other lower-carbon systems. This study demonstrated that a poorly-performing PET model can cause model bias which could substantially confound factors in studies investigating alternative scenarios in order to analyze their effect on TOC stocks.

RS is a solid proxy for yield when modeling soil C with RothC. The correlation between observed soybean yield and estimated VI values was high. Although the fit between observed and estimated corn yield was low, the resulting transformation of the estimated yield to C input was not significantly different and resulted in virtually no differences in RothC model outputs. However, although the technical aspect of this method is demonstrably acceptable, there are practical constraints given the potentially sparse availability of satellite images due to cloud interference and the relatively low temporal resolution of Landsat in particular. Additional satellite constellations could be included in future studies to help fill in data gaps, however, as more systems become established (Sentinel, SPOT, etc.). Limitations aside, the proven option to use RS for RothC input has tremendous implications in the scalability of the model's use to generate accurate estimates anywhere yields are not directly known, such as for regional or even national studies where crop classification and phenology maps are available.

Author Contributions

Ellen Maas: Conceptualization, Methodology, Formal analysis, Investigation, Writing – original draft, Visualization. Rattan Lal: Supervision, Funding acquisition.

Declaration of Competing Interest

The authors declare that they have no known competing financial interests or personal relationships that could have appeared to influence the work reported in this paper.

Acknowledgements

The School of Environment and Natural Resources of The Ohio State University, Columbus, Ohio financially supported this project. Support for this research was also provided by the NSF Long-term Ecological Research Program (DEB 1832042) at the Kellogg Biological Station and by Michigan State University AgBioResearch. Gratitude is extended to Kevin Coleman (Rothamsted Research, Harpenden,

575 Hertfordshire, England) and Yuki Hamada (Argonne National Laboratory, Lemont, IL) who provided
576 expert advice.

References

Amatya, D. M., R. W. Skaggs, and J. D. Gregory. 1995. “Comparison of Methods for Estimating REF-ET.” Journal of Irrigation and Drainage Engineering 121 (6): 427–35.

Asseng, S., F. Ewert, C. Rosenzweig, J. W. Jones, J. L. Hatfield, A. C. Ruane, K. J. Boote, et al. 2013. “Uncertainty in Simulating Wheat Yields under Climate Change.” Nature Climate Change 3 (9): 827–32.

Aune, J. and R. Lal 1997. “Agricultural productivity in the tropics and critical limits of properties of Oxisols, Ultisols and Alfisols.” Trop. Agric. (Trinidad) 74:96-103.

Austin, R. B., J. Bingham, R. D. Blackwell, L. T. Evans, M. A. Ford, C. L. Morgan, and M. Taylor. 1980. “Genetic Improvements in Winter Wheat Yields since 1900 and Associated Physiological Changes.” The Journal of Agricultural Science 94 (3): 675–89.

Awad, Mohamad M. 2019. “Toward Precision in Crop Yield Estimation Using Remote Sensing and Optimization Techniques.” Agriculture 9 (3): 54. https://doi.org/10.3390/agriculture9030054.

Baez-Gonzalez, A. D., J. R. Kiniry, S. J. Maas, M. L. Tiscareno, J. Macias C., J. L. Mendoza, C. W. Richardson, J. Salinas G., and J. R. Manjarrez. 2005. “Large-Area Maize Yield Forecasting Using Leaf Area Index Based Yield Model.” Agronomy Journal 97 (2): 418–25.

Balboa, G. R., V. O. Sadras, and I. A. Ciampitti. 2018. “Shifts in Soybean Yield, Nutrient Uptake, and Nutrient Stoichiometry: A Historical Synthesis-Analysis.” Crop Science 58 (1): 43–54.

601 Baveye, Philippe C., Laura Sophie Schnee, Pascal Boivin, Magdeline Laba, and Ricardo Radulovich. 2020.
602 “Soil Organic Matter Research and Climate Change: Merely Re-Storing Carbon Versus Restoring Soil
603 Functions.” Frontiers in Environmental Science 8: 161.
604
605 Blaney, H. F., and W. D. Criddle. 1962. “Determining Consumptive Use and Irrigation Water
606 Requirements.” USDA ARS Tech. Bull. 1275. Washington, D.C.
607
608 Bolinder, M. A., H. H. Janzen, E. G. Gregorich, D. A. Angers, and A. J. VandenBygaart. 2007. “An Approach
609 for Estimating Net Primary Productivity and Annual Carbon Inputs to Soil for Common Agricultural Crops
610 in Canada.” Agriculture, Ecosystems & Environment 118, no. 1–4 (January 2007): 29–42.
611
612 Bolton, Douglas K., and Mark A. Friedl. 2013. “Forecasting Crop Yield Using Remotely Sensed Vegetation
613 Indices and Crop Phenology Metrics.” Agricultural and Forest Meteorology 173 (May): 74–84.
614 https://doi.org/10.1016/j.agrformet.2013.01.007.
615
616 Bormann, H. 2011. “Sensitivity Analysis of 18 Different Potential Evapotranspiration Models to Observed
617 Climatic Change at German Climate Stations.” Climatic Change 104 (3): 729–53.
618
619 Chambers, A., R. Lal, and K. Paustian. 2016. “Soil Carbon Sequestration Potential of US Croplands and
620 Grasslands: Implementing the 4 per Thousand Initiative.” Journal of Soil and Water Conservation 71 (3):
621 68A-74A. https://doi.org/10.2489/jswc.71.3.68A.
622

623 Chao, Z., N. Liu, P. Zhang, T. Ying, and K. Song. 2019. “Estimation Methods Developing with Remote
624 Sensing Information for Energy Crop Biomass: A Comparative Review.” Biomass and Bioenergy 122
625 (March): 414–25. https://doi.org/10.1016/j.biombioe.2019.02.002.
626
627 Coleman, K., and D.S. Jenkinson. 2014. “RothC - A Model for the Turnover of Carbon in Soil.” Harpenden,
628 UK: Rothamsted Research.
629
630 Coleman, K., D. S. Jenkinson, G. J. Crocker, P. R. Grace, J. Klír, M. Körschens, P. R. Poulton, and D. D.
631 Richter. 1997. “Simulating Trends in Soil Organic Carbon in Long-Term Experiments Using RothC-26.3.”
632 Geoderma, Evaluation and Comparison of Soil Organic Matter Models, 81 (1): 29–44.
633
634 Comer, P. J, D. A. Albert, H. A. Wells, B. L. Hart, J. B. Raab, D. L. Prince, D. M. Kashian, R. A. Corner, and D.
635 W. Schuen. 1995. Michigan’s Native Landscape: As Interpreted from the General Land Office Surveys
636 1816-1856. Report to the U.S. E.P.A Water Division and the Wildlife Division. Lansing, MI: Michigan
637 Natural Features Inventory. 76 pp.
638
639 Crum, J. R. and H. P. Collins. 1995. KBS Soils. Kellogg Biological Station Long-term Ecological Research
640 Special Publication. Zenodo.
641
642 Dale, A., C. Fant, K. Strzepek, M. Lickley, and S. Solomon. 2017. “Climate Model Uncertainty in Impact
643 Assessments for Agriculture: A Multi-Ensemble Case Study on Maize in Sub-Saharan Africa.” Earth’s
644 Future 5 (3): 337–53.
645

de Jong, R., and P.M. Tugwood. 1987. “Comparison of Potential Evapotranspiration Models and Some Applications in Soil Water Modeling.” Canadian Agricultural Engineering 29 (1): 15-20.

de Mendiburu, F. 2021. “agricolae: Statistical Procedures for Agricultural Research.” R package version 1.3-5. https://CRAN.R-project.org/package=agricolae.

Droogers, P., and R. G. Allen. 2002. “Estimating Reference Evapotranspiration Under Inaccurate Data Conditions.” Irrigation and Drainage Systems Irrigation and Drainage Systems 16, no. 1 (2002): 33–45.

Ellert, B. H., and J. R. Bettany. 1995. “Calculation of Organic Matter and Nutrients Stored in Soils under Contrasting Management Regimes.” Canadian Journal of Soil Science 75 (4): 529–38. https://doi.org/10.4141/cjss95-075.

Gautam, S., U. Mishra, C. D. Scown, and Y. Zhang. 2020. “Sorghum Biomass Production in the Continental United States and Its Potential Impacts on Soil Organic Carbon and Nitrous Oxide Emissions.” GCB Bioenergy 12 (10): 878–90. https://doi.org/10.1111/gcbb.12736.

Gautam, S., U. Mishra, C. D. Scown, S. A. Wills, K. Adhikari, and B. A. Drewniak. 2022. “Continental United States May Lose 1.8 Petagrams of Soil Organic Carbon under Climate Change by 2100.” Global Ecology and Biogeography 31 (6): 1147–60. https://doi.org/10.1111/geb.13489.

Georgi, C., D. Spengler, S. Itzerott, and B. Kleinschmit. 2018. “Automatic Delineation Algorithm for Site-Specific Management Zones Based on Satellite Remote Sensing Data.” Precision Agriculture 19 (4): 684–707.

Goel, N. S. 1988. “Models of Vegetation Canopy Reflectance and Their Use in Estimation of Biophysical Parameters from Reflectance Data.” Remote Sensing Reviews 4 (1): 1–212.

Gollany, H.T., and R.W. Polumsky. 2018. “Simulating Soil Organic Carbon Responses to Cropping Intensity, Tillage, and Climate Change in Pacific Northwest Dryland.” Journal of Environmental Quality 47 (4): 625–34.

Gottschalk, P., J. U. Smith, M. Wattenbach, J. Bellarby, E. Stehfest, N. Arnell, T. J. Osborn, C. Jones, and P. Smith. 2012. “How Will Organic Carbon Stocks in Mineral Soils Evolve under Future Climate? Global Projections Using RothC for a Range of Climate Change Scenarios.” Biogeosciences 9 (8): 3151–71. https://doi.org/10.5194/bg-9-3151-2012.

Guo, D., S. Westra, and H. R. Maier. 2017. “Sensitivity of Potential Evapotranspiration to Changes in Climate Variables for Different Australian Climatic Zones.” Hydrology and Earth System Sciences 21 (4): 2107–26. https://doi.org/10.5194/hess-21-2107-2017.

Guo, L., P. Falloon, K. Coleman, B. Zhou, Y. Li, E. Lin, and F. Zhang. 2007. “Application of the RothC Model to the Results of Long-Term Experiments on Typical Upland Soils in Northern China.” Soil Use and Management 23 (1): 63–70.

Hargreaves, G. H. 1975. “Moisture Availability and Crop Production.” Transactions of the ASAE 18 (5): 0980–84.

694 Hargreaves, G. H., and Z. A. Samani. 1985. “Reference Crop Evapotranspiration from Temperature.”
695 Applied Engineering in Agriculture 1 (2): 96–99.
696
697 Hashimoto, S., M. Wattenbach, and P. Smith. 2011. “Litter Carbon Inputs to the Mineral Soil of Japanese
698 Brown Forest Soils: Comparing Estimates from the RothC Model with Estimates from MODIS.” Journal of
699 Forest Research 16 (1): 16–25.
700
701 Holben, B. N. 1986. “Characteristics of maximum-values composite images from temporal AVHRR data.”
702 Int. J. Remote Sens. 7:1417–1434.
703
704
705 Huete, A. R. 1988. “A Soil-Adjusted Vegetation Index (SAVI).” Remote Sensing of Environment 25: 295–
706 309.
707
708 Ines, Amor V. M., Narendra N. Das, James W. Hansen, and Eni G. Njoku. 2013. “Assimilation of Remotely
709 Sensed Soil Moisture and Vegetation with a Crop Simulation Model for Maize Yield Prediction.” Remote
710 Sensing of Environment 138 (November): 149–64. https://doi.org/10.1016/j.rse.2013.07.018.
711
712 Jenkinson, D. S. 1990. “The Turnover of Organic Carbon and Nitrogen in Soil.” Philosphical Transactions
713 of the Royal Society, B. 329: 361–68.
714
715 Jenny, H. 1961. E. W. Hilgard and the Birth of Modern Soil Science, Collana Della Rivista Agrochimica,
716 Pisa.
717

718 Jones, C., C. McConnell, K. Coleman, P. Cox, P. Falloon, D. Jenkinson, and D. Powlson. 2005. “Global
719 Climate Change and Soil Carbon Stocks; Predictions from Two Contrasting Models for the Turnover of
720 Organic Carbon in Soil.” Global Change Biology 11 (1): 154–66. https://doi.org/10.1111/j.1365-
721 2486.2004.00885.x.
722
723 Jones, J. R., C. S. Fleming, K. Pavuluri, M. M. Alley, M. S. Reiter, and W. E. Thomason. 2015. “Influence of
724 Soil, Crop Residue, and Sensor Orientations on NDVI Readings.” Precision Agriculture 16 (6): 690–704.
725
726 KBS. n.d. “MAIN CROPPING SYSTEM EXPERIMENT – MAIN SITE.” KBS LTER. Accessed February 4, 2020.
727 https://lter.kbs.msu.edu/research/long-term-experiments/main-cropping-system-experiment/.
728
729 Keel, S. G., J. Leifeld, J. Mayer, A. Taghizadeh-Toosi, and J. E. Olesen. 2017. “Large Uncertainty in Soil
730 Carbon Modelling Related to Method of Calculation of Plant Carbon Input in Agricultural Systems.”
731 European Journal of Soil Science 68 (6): 953–63.
732
733 Kemper, W. D., E. J. Koch, and United States Department of Agriculture. 1966. “Aggregate Stability of
734 Soils from Western United States and Canada; Measurement Procedure, Correlations with Soil
735 Constituents.” Washington: Agricultural Research Service, U.S. Dept. of Agriculture; [for sale by the Supt.
736 of Docs., U.S. Govt. Print. Off.], 1966.
737
738 Lal, R. 2004. “Soil carbon sequestration impacts on global climate change and food
739 security.” Science 304:1623. doi: 10.1126/science.1097396
740
741 Lal, R. 2016. “Beyond COP 21: Potential and Challenges of the ‘4 per Thousand’ Initiative.” Journal
742 of Soil and Water Conservation 71 (1): 20A-25A. https://doi.org/10.2489/jswc.71.1.20A.

Lal, R., W. Negassa, and K. Lorenz. 2015. “Carbon Sequestration in Soil.” Current Opinion in Environmental Sustainability, Environmental change issues, 15 (August): 79–86. https://doi.org/10.1016/j.cosust.2015.09.002.

Larocque, G. R., J. S. Bhatti, R. Boutin, and O. Chertov. 2008a. “Uncertainty Analysis in Carbon Cycle Models of Forest Ecosystems: Research Needs and Development of a Theoretical Framework to Estimate Error Propagation.” Ecological Modelling, The Importance of Uncertainty and Sensitivity Analysis in Process-based Models of Carbon and Nitrogen Cycling in Terrestrial Ecosystems with Particular Emphasis on Forest Ecosystems, 219 (3): 400–412. 177

Larocque, G. R., J. S. Bhatti, A. M. Gordon, N. Luckai, M. Wattenbach, J. Liu, C. Peng, et al. 2008b. “Chapter 18 - Uncertainty and Sensitivity Issues in Process-Based Models of Carbon and Nitrogen Cycles in Terrestrial Ecosystems.” In Developments in Integrated Environmental Assessment, edited by A. J. Jakeman, A. A. Voinov, A. E. Rizzoli, and S. H. Chen, 3:307–27. Environmental Modelling, Software and Decision Support. Elsevier.

Lee, J., J. W. Hopmans, D. E. Rolston, S. G. Baer, and J. Six. 2009. “Determining soil carbon stock changes: Simple bulk density corrections fail.” Agriculture, Ecosystems and Environment 134(3-4):251-56.

Liao, C., J. Wang, T. Dong, J. Shang, J. Liu, and Y. Song. 2019. “Using Spatio-Temporal Fusion of Landsat-8 and MODIS Data to Derive Phenology, Biomass and Yield Estimates for Corn and Soybean.” Science of The Total Environment 650 (February): 1707–21.

Liaqat, M. U., M. J. M. Cheema, W. Huang, T. Mahmood, M. Zaman, and M. M. Khan. 2017. “Evaluation of MODIS and Landsat Multiband Vegetation Indices Used for Wheat Yield Estimation in Irrigated Indus Basin.” Computers and Electronics in Agriculture 138 (June): 39–47.

Liu, J., E. Pattey, J. R. Miller, H. McNairn, A. Smith, and B. Hu. 2010. “Estimating Crop Stresses, Aboveground Dry Biomass and Yield of Corn Using Multi-Temporal Optical Data Combined with a Radiation Use Efficiency Model.” Remote Sensing of Environment 114 (6): 1167–77.

Lu, J., G. Sun, S. G. McNulty, and D. M. Amatya. 2005. “A Comparison of Six Potential Evapotranspiration Methods for Regional Use in the Southeastern United States1.” JAWRA Journal of the American Water Resources Association 41 (3): 621–33. https://doi.org/10.1111/j.1752-1688.2005.tb03759.x.

Lugato, E., A. Leip, and A. Jones. 2018. “Mitigation Potential of Soil Carbon Management Overestimated by Neglecting N_2O Emissions.” Nature Climate Change 8 (3): 219–23. https://doi.org/10.1038/s41558-018-0087-z.

Maas, E. D. V. L., R. Lal, K. Coleman, A. Montenegro, and W. A. Dick. 2017. “Modeling Soil Organic Carbon in Corn (Zea Mays L.)-Based Systems in Ohio under Climate Change.” Journal of Soil and Water Conservation 72, no. 3 (June 2017): 191–204.

Maas, S. J. 1988. “Using Satellite Data to Improve Model Estimates of Crop Yield.” Agronomy Journal 80 (4): 655–62.

Maresma, Angel, Lindsay Chamberlain, Aristotelis Tagarakis, Tulsi Kharel, Greg Godwin, Karl J. Czymmek, Elson Shields, and Quirine M. Ketterings. 2020. “Accuracy of NDVI-Derived Corn Yield Predictions Is Impacted by Time of Sensing.” Computers and Electronics in Agriculture 169 (February): 105236.

Martin, J. H, and W. H. Leonard. 1949. Principles of Field Crop Production. New York: Macmillan Company.

Marshall, M., K. Tu, and J. Brown. 2018. “Optimizing a Remote Sensing Production Efficiency Model for Macro-Scale GPP and Yield Estimation in Agroecosystems.” Remote Sensing of Environment 217 (November): 258–71. https://doi.org/10.1016/j.rse.2018.08.001.

Masek, J. G., E. F. Vermote, N. Saleous, R. Wolfe, F. G. Hall, F. Huemmrich, F. Gao, J. Kutler, and T. K. Lim, 2006. A Landsat surface reflectance data set for North America, 1990-100, IEEE Geoscience and Remote Sensing Letters. 3:68-72.

Matthews, H. D., K. Zickfeld, M. Dickau, A. J. MacIsaac, S. Mathesius, C. Nzotungicimpaye, and A. Luers. 2022. “Temporary Nature-Based Carbon Removal Can Lower Peak Warming in a Well-below 2 °C Scenario.” Communications Earth & Environment 3 (1): 1–8. https://doi.org/10.1038/s43247-022-00391-z.

Menne, M. J., I. Durre, B. Korzeniewski, S. McNeal, K. Thomas, X. Yin, S. Anthony, R. Ray, R. S. Vose, B. E. Gleason, and T. G. Houston. 2012a. Global Historical Climatology Network - Daily (GHCN-Daily), Version 3. Daily Summaries. NOAA National Climatic Data Center. Accessed: June 18, 2019.

814 Menne, M. J., I. Durre, R. S. Vose, B. E. Gleason, and T. G. Houston. 2012b. An Overview of the Global
815 Historical Climatology Network-Daily Database. J. Atmos. Oceanic Technol., 29, 897-910.
816 Monteith, J. L. 1965. “Evaporation and Environment.” Symposia of the Society for Experimental Biology
817 19: 205–34.
818
819 Monteith, J. L. 1965. “Evaporation and Environment.” Symposia of the Society for Experimental Biology
820 19: 205–34.
821
822 Moreno, F., J. M. Murillo, F. Pelegrín, and I. F. Girón. 2006. “Long-Term Impact of Conservation Tillage on
823 Stratification Ratio of Soil Organic Carbon and Loss of Total and Active CaCO3.” Soil and Tillage Research
824 85 (1): 86–93.
825
826 Panek, E., D. Gozdowski, M. Stępień, S. Samborski, D. Ruciński, and B. Buszke. 2020. “Within-Field
827 Relationships between Satellite-Derived Vegetation Indices, Grain Yield and Spike Number of Winter
828 Wheat and Triticale.” Agronomy 10 (11): 1842. https://doi.org/10.3390/agronomy10111842.
829
830 Penman, H. L., and B. A. Keen. 1948. “Natural Evaporation from Open Water, Bare Soil and Grass.”
831 Proceedings of the Royal Society of London. Series A. Mathematical and Physical Sciences 193 (1032):
832 120–45.
833
834 Priestley, C. H. B., and R. J. Taylor. 1972. “On the Assessment of Surface Heat Flux and Evaporation Using
835 Large-Scale Parameters.” Monthly Weather Review 100 (2): 81–92.
836

837 Prince, S. D., J. Haskett, M. Steininger, H. Strand, and R. Wright. 2001. “Net Primary Production of U.S.
838 Midwest Croplands from Agricultural Harvest Yield Data.” Ecological Applications 11 (4): 1194.
839
840 Qi, J., A. Chehbouni, A. R. Huete, Y. H. Kerr, and S. Sorooshian. 1994a. “A Modified Soil Adjusted
841 Vegetation Index.” Remote sensing of environment 48 (2): 119.
842
843 Qi, J., Y. Kerr, and A. Chehbouni. 1994b. “External factor consideration in vegetation index
844 development.” Proc. of Physical Measurements and Signatures in Remote Sensing, ISPRS, 723-730.
845 Rondeaux, G., M. Steven, and F. Baret. 1996. “Optimization of Soil-Adjusted Vegetation Indices.”
846 Remote Sensing of Environment 55 (2): 95–107.
847
848 Quarmby, N.A., M. Milnes, T.L. Hindle, and N. Silleos. 1993. “The Use of Multi-Temporal NDVI
849 Measurements from AVHRR Data for Crop Yield Estimation and Prediction.” International Journal of
850 Remote Sensing 14 (2): 199–210.
851
852 R Core Team. 2019. R: A language and environment for statistical computing. R Foundation for Statistical
853 Computing, Vienna, Austria. URL https://www.R-project.org/.
854
855 Ranatunga, K., M.J. Hill, M.E. Probert, and R.C. Dalal. 2001. “Comparative Application of APSIM, RothC
856 and Century to Predict Soil Carbon Dynamics.” In Proceedings of the International Congress on
857 Modelling and Simulation (MODSIM’01), 733–38.
858

Riggers, C., C. Poeplau, A. Don, C. Bamminger, H. Höper, and R. Dechow. 2019. “Multi-Model Ensemble Improved the Prediction of Trends in Soil Organic Carbon Stocks in German Croplands.” Geoderma 345 (July): 17–30. https://doi.org/10.1016/j.geoderma.2019.03.014.

Roe, S., C. Streck, M. Obersteiner, S. Frank, B. Griscom, L. Drouet, O. Fricko, et al. 2019. “Contribution of the Land Sector to a 1.5 °C World.” Nature Climate Change 9 (11): 817–28. https://doi.org/10.1038/s41558-019-0591-9.

Rogelj, J., M. den Elzen, N. Höhne, T. Fransen, H. Fekete, H. Winkler, R. Schaeffer, F. Sha, K. Riahi, and M. Meinshausen. 2016. “Paris Agreement Climate Proposals Need a Boost to Keep Warming Well below 2 °C.” Nature 534 (7609): 631–39. https://doi.org/10.1038/nature18307.

Roux, S., F. Brun, and D. Wallach. 2014. “Combining Input Uncertainty and Residual Error in Crop Model Predictions: A Case Study on Vineyards.” European Journal of Agronomy 52 (January): 191–97.

Sakamoto, T., M. Yokozawa, H. Toritani, M. Shibayama, N. Ishitsuka, and H. Ohno. 2005. “A Crop Phenology Detection Method Using Time-Series MODIS Data.” Remote Sensing of Environment 96 (3): 366–74.

Sentelhas, P. C., T. J. Gillespie, and E. A. Santos. 2010. “Evaluation of FAO Penman–Monteith and Alternative Methods for Estimating Reference Evapotranspiration with Missing Data in Southern Ontario, Canada.” Agricultural Water Management 97 (5): 635–44.

882 Sharma, Meenakshi, Rajesh Kaushal, Prashant Kaushik, and Seeram Ramakrishna. 2021. “Carbon
883 Farming: Prospects and Challenges.” Sustainability 13 (19): 11122.
884 https://doi.org/10.3390/su131911122.
885
886 Sinclair, T. R. 1998. “Historical Changes in Harvest Index and Crop Nitrogen Accumulation.” Crop Science
887 38 (3): 638–43.
888
889 Sun, D., Y. Yu, and M. D. Goldberg. 2011. “Deriving Water Fraction and Flood Maps From MODIS Images
890 Using a Decision Tree Approach.” IEEE Journal of Selected Topics in Applied Earth Observations and
891 Remote Sensing 4 (4): 814–25.
892
893 Tate, K.R., D.J. Ross, T.W. Speir, and P.B.S. Hart. 1985. “Soil - the fundamental life support system and its
894 disturbance by man.” In Proceedings of the soil dynamics and land use seminar (ed. I.B. Campbell), New
895 Zealand Society of Soil Science, and the New Zealand Soil Conservators Association, Blenheim Printing
896 Co., Blenheim, New Zealand, pp. 243.
897
898 Teal, R. K., B. Tubana, K. Girma, K. W. Freeman, D. B. Arnall, O. Walsh, and W. R. Raun. 2006. “In-Season
899 Prediction of Corn Grain Yield Potential Using Normalized Difference Vegetation Index.” Agronomy
900 Journal 98 (6): 1488–94.
901
902 Tegos, A., N. Malamos, A. Efstratiadis, I. Tsoukalas, A. Karanasios, and D. Koutsoyiannis. 2017.
903 “Parametric Modelling of Potential Evapotranspiration: A Global Survey.” Water 9 (10): 795.
904

905 Teixeira, Ricardo F. M., Tiago G. Morais, and Tiago Domingos. 2021. “Global Process-Based
906 Characterization Factors of Soil Carbon Depletion for Life Cycle Impact Assessment.” Scientific Data 8 (1):
907 237. https://doi.org/10.1038/s41597-021-01018-2.
908
909 The White House. 2021. “Long-Term Strategy of the United States, Pathways to Net-Zero.”
910 https://www.whitehouse.gov/wp-content/uploads/2021/10/US-Long-Term-Strategy.pdf. Accessed May
911 18, 2022.
912
913 Thenkabail, P. S., A. D. Ward, J. G. Lyon, and P. Van Deventer. 1992. “Landsat Thematic Mapper Indices
914 for Evaluating Management and Growth Characteristics of Soybeans and Corn.” Transactions of the
915 ASAE 35 (5): 1441–48.
916
917 Thornthwaite, C. W. 1948. “An Approach toward a Rational Classification of Climate.” Geographical
918 Review 38 (1): 55–94.
919
920 Thornthwaite, C. W. and J. R. Mather. 1955. The Water Balance. Publications in Climatology, Vol 8, No. 1,
921 Centerton, N.J., Laboratory of Climatology.
922
923 Todd-Brown, K. E. O., J. T. Randerson, W. M. Post, F. M. Hoffman, C. Tarnocai, E. a. G. Schuur, and S. D.
924 Allison. 2013. “Causes of Variation in Soil Carbon Simulations from CMIP5 Earth System Models and
925 Comparison with Observations.” Biogeosciences 10 (3): 1717–36.
926

927 Todd-Brown, K., B. Zheng, and T. W. Crowther. 2018. “Field-Warmed Soil Carbon Changes Imply High
928 21st-Century Modeling Uncertainty.” Biogeosciences 15 (12): 3659–71. https://doi.org/10.5194/bg-15-
929 3659-2018.
930
931 Tomecek, M. and G. P. Robertson. 1996. Land Use History for the Kellogg Biological Station and
932 Surrounding Area. Kellogg Biological Station Long-term Ecological Research Special Publication. Zenodo.
933
934 Todorovic, G. R., M. Stemmer, M. Tatzber, C. Katzlberger, H. Spiegel, F. Zehetner, and Martin H.
935 Gerzabek. 2010. “Soil-Carbon Turnover under Different Crop Management: Evaluation of RothC-Model
936 Predictions under Pannonian Climate Conditions.” Journal of Plant Nutrition and Soil Science 173 (5):
937 662–70.
938
939 Tucker, C. J. 1980. “A Critical Review of Remote Sensing and Other Methods for Non-Destructive
940 Estimation of Standing Crop Biomass.” Grass and Forage Science 35 (3): 177–82.
941 https://doi.org/10.1111/j.1365-2494.1980.tb01509.x.
942
943 Uri, N. D. 2001. “The potential impact of conservation practices in US agriculture on global climate
944 change.” Journal of Sustainable Agriculture 18(1):109-31.
945
946 U.S. Department of Agriculture, National Agricultural Statistics Service (USDA-NASS). 2019. Census of
947 Agriculture-United States Data. Available online: https://www.nass.usda.gov/AgCensus/index.php.
948
949 U.S. Geological Survey (USGS). n.d.(a). “EarthExplorer - Home.” Accessed April 15, 2019.
950 https://earthexplorer.usgs.gov/.

U.S. Geological Survey (USGS). n.d.(b). “Landsat Surface Reflectance-Derived Spectral Indices.” Accessed February 26, 2020. https://www.usgs.gov/land-resources/nli/landsat/landsat-surface-reflectance-derived-spectral-indices?qt-science_support_page_related_con=0#qt-science_support_page_related_con.

U.S. Geological Survey (USGS). 2017. “ESPA - LSRD.” October 25, 2017. Accessed August 15, 2019. https://espa.cr.usgs.gov/.

Van Bavel, C. H. M. 1966. “Potential Evaporation: The Combination Concept and Its Experimental Verification.” Water Resources Research 2 (3): 455–67.

Wang, G., and S. Chen. 2012. “A Review on Parameterization and Uncertainty in Modeling Greenhouse Gas Emissions from Soil.” *Geoderma* 170 (January): 206–16.

Wang, R., K. Cherkauer, and L. Bowling. 2016. “Corn Response to Climate Stress Detected with Satellite-Based NDVI Time Series.” Remote Sensing 8 (4): 269. https://doi.org/10.3390/rs8040269.

Watanabe, S., T. Hajima, K. Sudo, T. Nagashima, T. Takemura, H. Okajima, T. Nozawa, et al. 2011. “MIROC-ESM 2010: Model Description and Basic Results of CMIP5-20c3m Experiments.” Geoscientific Model Development 4 (4): 845–72. https://doi.org/10.5194/gmd-4-845-2011.

West, L., S. Wills, and T. Loecke. 2013. Rapid assessment of US Soil Carbon (RaCA) for climate change and conservation planning: Summary of soil carbon stocks for the conterminous United States. Washington, DC: U.S. Department of Agriculture, Natural Resources Conservation Service.

Wutzler, T., and M. Reichstein. 2007. “Soils Apart from Equilibrium - Consequences for Soil Carbon Balance Modelling.” Biogeosciences 4 (1): 125–36.

Yang, C., and J. H. Everitt. 2012. “Using Spectral Distance, Spectral Angle and Plant Abundance Derived from Hyperspectral Imagery to Characterize Crop Yield Variation.” Precision Agriculture 13 (1): 62–75.

Yokozawa, M., Y. Shirato, T. Sakamoto, S. Yonemura, M. Nakai, and T. Ohkura. 2010. “Use of the RothC Model to Estimate the Carbon Sequestration Potential of Organic Matter Application in Japanese Arable Soils.” Soil Science and Plant Nutrition 56 (1): 168–76.

Zhao, H., Z. Yang, L. Di, L. Li, and H. Zhu. 2009. “Crop Phenology Date Estimation Based on NDVI Derived from the Reconstructed MODIS Daily Surface Reflectance Data.” In 2009 17th International Conference on Geoinformatics, 1–6.

Zhu, Xiaolin, and Desheng Liu. 2015. “Improving Forest Aboveground Biomass Estimation Using Seasonal Landsat NDVI Time-Series.” ISPRS Journal of Photogrammetry and Remote Sensing 102 (April): 222–31. https://doi.org/10.1016/j.isprsjprs.2014.08.014.